bubbles exposed at either surface. Two methods were used for vacuum extraction of the gases. Samples A1 and A2 were cracked open by thermal stress from an external hot-air blast: in sample C2 the gas was removed by partial melting and ultrasonic extraction from the meltwater. The gas contents of the three ~100-g pieces were ~1.2, 1.1, and 0.64 cm^3 (STP), but, because these pieces were cut to exclude bubbles in long channels open to air, we collected only a fraction of the original gas in each piece of ice. The GC techniques and analytical precision are described in note 14 of (*4*).

7. In Eq. 1, C_i^0, the initial gas content of a kilogram of water, is partitioned during the freezing process between gas and liquid phases by the equilibrium condition: $C_i = \beta_i \cdot p_i$, where C_i is the concentration in the liquid and p_i is the partial pressure of gas i in the bubbles, given by $X_i \cdot P_G$. The two terms on the right side of Eq. 1 are therefore the amounts of gas i in solution and in bubbles, expressed in cubic centimeters at standard temperature and pressure (cm^3 STP) per kilogram of original fluid. Because only ratios are plotted in Fig. 2, all equilibrium abiogenic systems should follow the gas and liquid trajectories given by these curves (except for slight deviations due to mixing): however, waters that have been partially outgassed or mixed with supersaturated waters will produce bubbles that begin on the curve somewhere below the initial "air point" and arrive at a given composition with lower values of ψ and larger values of F_L than in the case of initial saturation equilibrium. Nevertheless, the biogenic systems will follow parallel trajectories, offset to higher O_2/Ar ratios by displacements proportional to the input of O_2 by net biological production.
8. C. P. McKay *et al.*, *Nature* **313**, 561 (1985).
9. Z. Top, S. Martin, P. Becker, *Geophys. Res. Lett.* **12**, 821 (1985).
10. R. F. Weiss, *Deep-Sea Res.* **17**, 721 (1970).
11. Trajectories 1 and 2 in Fig. 2 can be described in terms of an initial mass of 1 kg of meltwater with $C^*_{O_2}$ = 10.22 cm^3 (STP), (σ_O = 1) at the ψ = 0 point. On curve 1 the mass of water is reduced by freezing to 200 g of liquid water containing 4.10 cm^3 (STP) of O_2, with σ_O = 2.00. Photosynthesis (J) then produces 0.50 cm^3 of additional O_2, or 11% of the total O_2 content of the water, with a final σ_O = 2.25. Trajectory 2 follows an addition of 1.23 cm^3 (STP) of photosynthetic O_2 to the original 1 kg of water and 10.22 cm^3 of atmospheric O_2, so that the biologic fraction is again 11% of the total dissolved O_2. Freezing along curve 2 then produces 200 g of residual water, with 4.60 cm^3 of O_2 and σ_O = 2.25. All other trajectories (for example, curve 3) produce a similar final state of the system.
12. We thank D. Burtner for the GC measurements; D. Andersen, L. Leary, and D. Schwindler for field assistance to R.A.W. and C.P.M.; and E. Hernandez for maintaining the Isotope Laboratory at Scripps Institution of Oceanography (SIO). Work at SIO was supported by NSF grant DPP87-22718 and National Aeronautics and Space Administration (NASA) grant NAGW-972. Work at the Desert Research Institute and Ames Research Center was supported by NSF grant DPP84-16340 and NASA grant NCA2-182.

28 October 1991; accepted 30 October 1991

The Earth's Angular Momentum Budget on Subseasonal Time Scales

J. O. DICKEY, S. L. MARCUS, J. A. STEPPE, R. HIDE

Irregular length of day (*LOD*) fluctuations on time scales of less than a few years are largely produced by atmospheric torques on the underlying planet. Significant coherence is found between the respective time series of *LOD* and atmospheric angular momentum (*AAM*) determinations at periods down to 8 days, with lack of coherence at shorter periods caused by the declining signal-to-measurement noise ratios of both data types. Refinements to the currently accepted model of tidal Earth rotation variations are required, incorporating in particular the nonequilibrium effect of the oceans. The remaining discrepancies between *LOD* and *AAM* in the 100- to 10-day period range may be due to either a common error in the *AAM* data sets from different meteorological centers, or another component of the angular momentum budget.

THE ROTATION VECTOR $\boldsymbol{\Omega}(t)$ OF THE solid Earth (where t denotes time and solid Earth refers to the crust and the mantle) with which the solid Earth rotates relative to a frame of reference defined by the fixed stars exhibits complicated changes of up to several parts in 10^8 in speed, corresponding to variations of several milliseconds in the length of day (*LOD*), $\Lambda(t)$. These changes occur over a broad spectrum of time scales and are manifestations of (i) changes in the inertia tensor of the solid Earth associated with redistribution of matter within it, and (ii) the action of applied torques. These torques are primarily produced by gravitational action of the moon, sun, and planets and by motions in the underlying liquid core and overlying oceans and atmosphere (*1*).

Irregular *LOD* fluctuations on time scales less than a few years are largely produced by atmospheric torques (*1–5*); concomitant stresses on the solid Earth are applied directly over continental regions and indirectly over the oceans. If the angular momentum of the solid Earth is $\mathbf{H}^{(s)}$ and $\mathbf{L}$ is the applied torque, then $\dot{\mathbf{H}}^{(s)}$, the time rate of change of $\mathbf{H}^{(s)}$ in an inertial frame satisfies

$$\dot{\mathbf{H}}^{(s)} = \mathbf{L} \quad (1)$$

It is convenient to write

$$\mathbf{L} = -\dot{\mathbf{H}}^{(a)} + \mathbf{l} \quad (2a)$$

and

$$\mathbf{l} = \mathbf{l}_{ext} - \dot{\mathbf{H}}^{(o)} - \dot{\mathbf{H}}^{(c)} \quad (2b)$$

where $\mathbf{H}^{(a)}$ is the total angular momentum of the atmosphere, so that $\mathbf{l}$ is the difference between (i) torques acting upon the whole Earth associated with external gravitational effects ($\mathbf{l}_{ext}$) and (ii) torques associated with angular momentum fluctuations in the oceans [$\dot{\mathbf{H}}^{(o)}$] and core [$\dot{\mathbf{H}}^{(c)}$]. The angular momentum budget between the atmosphere and solid Earth is then

$$\dot{\mathbf{H}}^{(s)} = -\dot{\mathbf{H}}^{(a)} + \mathbf{l} \quad (3)$$

Investigations into the Earth's angular momentum budget and research into solid Earth-atmosphere interactions have been revolutionized by the advent of modern space geodetic measurements of the Earth's rotation. These advances have been accompanied by improvements in measurements and numerical models of the Earth's global atmosphere, which are used to calculate the atmospheric angular momentum (*AAM*). The most progress has been made in investigations concerned with the axial component of Eq. 3, in which *LOD* fluctuations reflecting changes in the axial component $H_3^{(s)}$ of $\mathbf{H}^{(s)}$ are compared with fluctuations in the axial component $H_3^{(a)}$ of $\mathbf{H}^{(a)}$ (Fig. 1).

The present paper extends these studies down to periods of a few days, thereby improving the limits that can be placed on the magnitude of l_3 on these time scales. A nonzero value of l_3 greater than the errors involved in its determination would be a measure of the extent to which angular momentum fluctuations in other components of the system (such as the oceans) have to be taken into account at these high frequencies (assuming that external gravitational effects are properly accounted for). Hence, a comparison between *AAM* and *LOD* at these higher frequencies could uncover the ocean's role and further elucidate our understanding of the interaction between the solid Earth and the atmosphere.

The observed *LOD* time series can conveniently be separated into four components (*2*): (i) a constant term Λ_0 = 86,400 s representing the standard length-of-day, (ii) strictly periodic

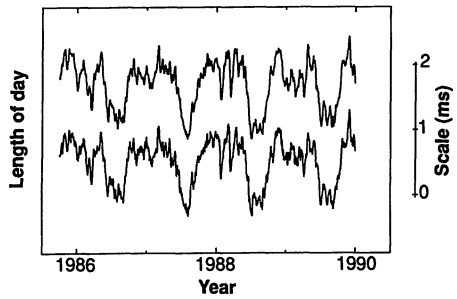

Fig. 1. Time series of LOD*, as determined by the Kalman-filtered combined space geodetic data (top) and from the combined *AAM* data (bottom); a 1-year moving average has been removed from both series. Tidal terms (*18*) have been removed from *LOD*.

J. O. Dickey, S. L. Marcus, J. A. Steppe, Jet Propulsion Laboratory, California Institute of Technology, 4800 Oak Grove Drive, Pasadena, CA 91109.
R. Hide, Robert Hooke Institute, The Observatory, Clarendon Laboratory, Parks Road, Oxford OX1 3PU, England, U.K.

variations $\Lambda_1(t)$ of up to about 0.5 ms due to tidally induced changes in the inertia tensor of the Earth at known tidal frequencies, (iii) a steady increase of 1.4 ms per century associated with tidal friction (Λ_2), and (iv) the residual time series $\Lambda^*(t)$, which fluctuates irregularly on all time scales. The axial component of the *AAM* is conventionally expressed in terms of the dimensionless effective atmospheric angular momentum function χ_3, given by

$$\chi_3(t) \equiv \frac{0.70R^4}{gC}\int_{-\pi/2}^{\pi/2}\int_0^{2\pi} p_s \cos^3\phi d\lambda d\phi + \frac{R^3}{gC\Omega}\int_0^{p_s}\int_{-\pi/2}^{\pi/2}\int_0^{2\pi} u\cos^2\phi d\lambda d\phi dp \quad (4)$$

where (ϕ,λ) denote latitude and longitude, respectively, $p_s(\phi,\lambda,t)$ is the surface pressure, $u(\phi,\lambda,p,t)$ is the eastward (westerly) component of the wind velocity relative to Earth's surface at (ϕ,λ) and pressure level p, R is the mean radius of the Earth (6.37×10^6 m), $g = 9.81$ m s^{-2} is the mean acceleration due to gravity, Ω is the standard rotation rate of Earth (7.292115×10^{-5} rad s^{-1}), and $C = 7.04 \times 10^{37}$ kg m^2 is the polar moment of inertia of the crust and mantle (which is about 10 times that of the core, 3000 times that of the oceans, and 10^6 times that of the atmosphere) (*3*). The coefficient 0.70 incorporates the so-called "Love number" correction, which allows for changes in the polar moment of inertia of the mantle due to the Earth's elastic response to surface pressure changes (*3*). When budget calculations are expressed in terms of $\Lambda(t)$ and $X(t)$ [where $X(t)$ is χ_3 expressed in units of time; see (*5*)], the axial component of Eq. 3 gives

$$\dot{\Lambda}^*(t) = \dot{X}(t) + \dot{x}(t) \quad (5)$$

where by definition $\dot{x}(t)$ measures the axial component of the nonatmospheric torque.

In the mid-1980's, significant coherence between *LOD* and *AAM* was established down to periods of 40 days through the joint analysis of meteorological data from the U.S. National Meteorological Center (NMC) and Earth rotation data from optical astrometry and Lunar Laser Ranging (LLR); data from the period 1976 to 1981 were considered (*5*). This limit was later reduced to 14 days by use of NMC *AAM* data and the nearly daily IRIS (International Radio Interferometric Surveying) Intensive VLBI (Very Long Baseline Interferometry) measurements for 1985 to 1988 (*6*). Further analysis reduced their limit to 10 days (*7*).

We considered two length-of-day data sets: the IRIS Intensive Earth Rotation Measurements and the JPL Kalman-smoothed series. The IRIS Intensive measurements are based on nearly daily VLBI observations that began on a routine operational basis in April 1985 (*8*); we used data from April 1985 through June 1990. The JPL Kalman-filtered series combines Earth rotation results from VLBI and LLR to form a high-quality series in which the effects of reference frames and the unevenness of data quality and quantity have been addressed (*9*); we used the series from April 1985 through June 1990. Also used were *AAM* data sets from four meteorological centers: The NMC (*10*), the European Centre for Medium Range Weather Forecasts (EC) (*11*), the Japan Meteorological Agency (JMA) (*12*), and the United Kingdom Meteorological Office (UKMO) (*13*). Both the wind term and pressure contribution without the inverted barometer (IB) assumption (pressure contribution with the IB assumption is not available from all centers) were included in the *AAM*. Intercomparison studies (*14, 15*) have shown that these meteorological series are in excellent agreement. The subannual variations in *LOD* and the average of the four *AAM* series (combined *AAM*) track each other closely (Fig. 1).

We first address the angular momentum budget by utilizing coherence analysis (*5, 16*) between the Kalman-filtered *LOD** and the combined *AAM*. Results (Fig. 2A) using a relatively narrow spectral smoothing to form the coherence estimate (*5*) indicate that significant coherence between these two series is lost at ~15 days, similar to other recent findings (*6*). The threshold level above which a coherence estimate is significantly different from zero depends on the width of the spectral smoothing used, while the expected value of the coherence estimate does not depend appreciably on the smoothing. A higher degree of spectral smoothing [for example, 11 bins (1 bin = 0.0005 cycles per day) in Fig. 2B versus 5 bins in Fig. 2A] indicates that coherence is significant down to ~8 days, with the exception of a dip near the 13.6-day tidal period. Significant coherence also extends down to 8 days when the IB correction (available from the JMA and the NMC) is used, although coherence is lost at 10 days when the pressure term is neglected completely.

An alternative approach is to model the expected coherence as a function of frequency using stochastic models of the geophysical processes and of the measurement errors involved. We assume for subseasonal periods that both the *LOD** and *AAM* data sets are composed of a common geophysical signal, S, and noise components, N_L and N_A, respectively, assumed to be uncorrelated with the signal and with each other:

$$LOD^* = \Lambda^*(t) = S + N_L \quad (6)$$

$$AAM = X(t) = S + N_A \quad (7)$$

The squared coherence between the two series is then

$$coh^2 = (1 + E_L/P)^{-1}(1 + E_A/P)^{-1} \quad (8)$$

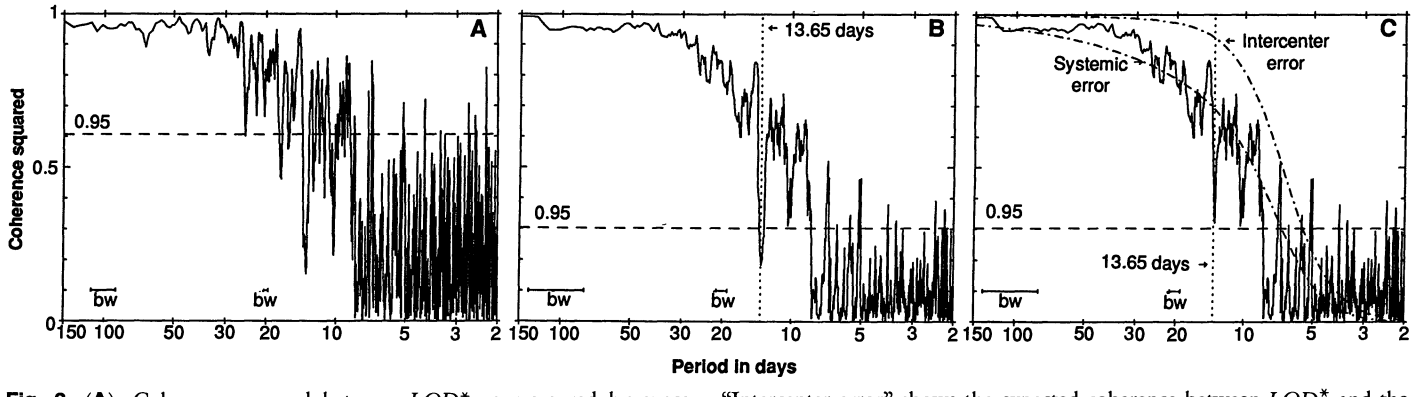

Fig. 2. (**A**). Coherence squared between *LOD** as measured by space geodetic techniques (*9*), and that inferred from the combined *AAM* data, with a spectral smoothing of 5 [the Yoder *et al.* (*18*) model has been used to remove the effect of *LOD* variations induced by the tides]; (**B**) same as (A) except with a spectral smoothing of 11; (**C**) same as (B) except that the Brosche *et al.* (*19*) tidal model has been utilized. The curve labeled as "Intercenter error" shows the expected coherence between LOD_I^* and the combined *AAM* for the model of the *AAM* error spectrum based on the *AAM* pairwise differences (Fig. 3B); also shown is the expected coherence between the two series based on the combined *AAM-LOD* difference (Fig. 3D, labeled as "Systematic error"). Horizontal dashed line is 95% confidence level; bw is the bandwidth.

where P is the signal power spectral density (*PSD*) $\langle S, S\rangle$, and E is the noise *PSD* $\langle N, N\rangle$. If power laws with known exponents are assumed for the power spectral density of the signal and the noise, one can determine the coherence for all frequencies by estimating the signal-to-noise ratio (*SNR*) for each series (P/E_L and P/E_A) at some standard period, taken here to be 10 days.

At subseasonal frequencies, the *LOD** (Λ^*) may be adequately modeled as a random walk, which implies that $P \propto f^{-2}$ [see (*5*)]. The axial component of Earth rotation is monitored by measuring universal time (*UT1*), the instantaneous angle of the Earth relative to an inertial reference frame. Assuming the successive *UT1* measurement errors are statistically independent, the measurement error spectrum for *UT1* is white (that is, no dependence on the frequency). The noise component N_L of the *LOD* series, derived from *UT1* by time differentiation, therefore, is "blue" noise (that is, $E_L \propto f^2$). Any procedure for computing an *LOD* series from a discrete series of *UT1* data imposes some smoothing on the blue measurement noise in *LOD* as well as on the *LOD* signal. In order to more clearly display the *PSD* and *LOD* measurement noise, and to maximize cancellation of the common component when forming *LOD-AAM*, it is desirable to minimize this smoothing. For this purpose we used a special Kalman smoothing of the IRIS Intensive *UT1* values that had the measurement uncertainties made vanishingly small. The transfer function of this special filtering can be roughly modeled as a simple interpolation (*17*). Changing the measurement formal error merely changes the filter transfer function (see *17*), and coherence is not affected by a linear filtering of either process.

The *PSD* of this specially filtered *LOD** series derived from the IRIS Intensive *UT1* data, called LOD_I^*, is modeled as:

$$\left\langle LOD_I^*, LOD_I^* \right\rangle = \left[P_o \left(\frac{f}{f_o}\right)^{-2} + E_{LO}\left(\frac{f}{f_o}\right)^2 \right] \times \left(\frac{\sin \pi f dt}{\pi f dt}\right)^2 \quad (9)$$

where P_o is the signal *PSD* at f_o [taken here to be $(10 \text{ days})^{-1}$], E_{LO} is the LOD_I^* noise PSD at f_o and dt is the effective interpolation time between neighboring data points in the observed *UT1* data, typically 1 or 2 days [see (*17*)]. The inverse square power law, with a standard coefficient P_o of 0.0182 ms^2 per cycle per day from the JPL Kalman filter (*9*), shows a good fit to the spectrum of the LOD_I^* data down to ~15 days (Fig. 3A). As shown below, the excess spectral power at periods near 14 days results largely from inaccuracies in the standard tidal model (see Figs. 3D and 5), whereas at higher frequencies, the noise term begins to make a sizable contribution. The *SNR*, P_o/E_{LO}, is taken to be 5.0 at 10 days, corresponding to a *UT1* measurement error (standard deviation) of about 0.07 ms over the time frame involved; the formal errors claimed for the IRIS Intensive *UT1* data average ~0.06 ms over this time period. For dt = 1.75 days, the *LOD* model with these parameters fits the LOD_I^* spectrum well from periods of 150 days down to 2 days (Fig. 3A).

The *AAM*, like *LOD**, is suitably modeled by a random walk ($P \propto f^{-2}$) [see (*5*)]. The spectra of the differences among the *AAM* series from the JMA, NMC, and UKMO (all available at 00Z) (Fig. 3B), however, behave as flicker noise (spectral index of −1) over the period range of 150 to 2 days. We therefore modeled the *AAM* noise as $E_A \propto f^{-1}$. The *PSD* of the *AAM* data (Fig. 3C) is modeled as $P_o(f/f_o)^{-2} + E_{AO}(f/f_o)^{-1}$, where P_o is the same value used in modeling the *LOD** spectrum. Although the *AAM* spectra show some evidence for attenuation at high frequencies, the simple arguments used to suggest a model for the *LOD* attenuation [see (*16*)] are not directly applicable, so no attenuation factor was applied to the *AAM* model.

The spectrum of the difference between LOD_I^* and the combined *AAM* (Fig. 3D) shows that the power varies approximately as f^{-1} at periods longer than about 15 days. This relation suggests that *AAM* noise dominates the LOD_I^*-*AAM* spectrum in this frequency range. If the measurement errors in the different *AAM* data sets are statistically independent and identically distributed, the *PSD* of the error in each is lower than the *PSD* of the difference of two sets by a factor of 2. The *PSD* of the difference of about 0.0045 ms^2 per cycle per day at 10 days (Fig. 3B) is indicative of a *SNR*, P_o/E_{AO}, for the individual *AAM* series of 8.2 at 10 days, and the *PSD* of the error for the combined *AAM* series is a factor of 4 lower than that of the individual series. Thus, the *PSD* of LOD_I^*-*AAM* is modeled as

$$\frac{1}{4}E_{AO}\left(\frac{f}{f_o}\right)^{-1} + E_{LO}\left(\frac{f}{f_o}\right)^2\left(\frac{\sin \pi f dt}{\pi f dt}\right)^2 + P_o\left(\frac{f}{f_o}\right)^{-2}\left(\frac{\sin \pi f dt}{\pi f dt} - 1\right)^2 \quad (10)$$

where the last term is insignificant. This *PSD* model ("intercenter" in Fig. 3D), clearly cannot account for the magnitude of the LOD_I^*-*AAM* residual. Attempting to explain the residual at periods longer than, say, 10 days as due to a systematic error in *LOD* would require an unreasonable level of

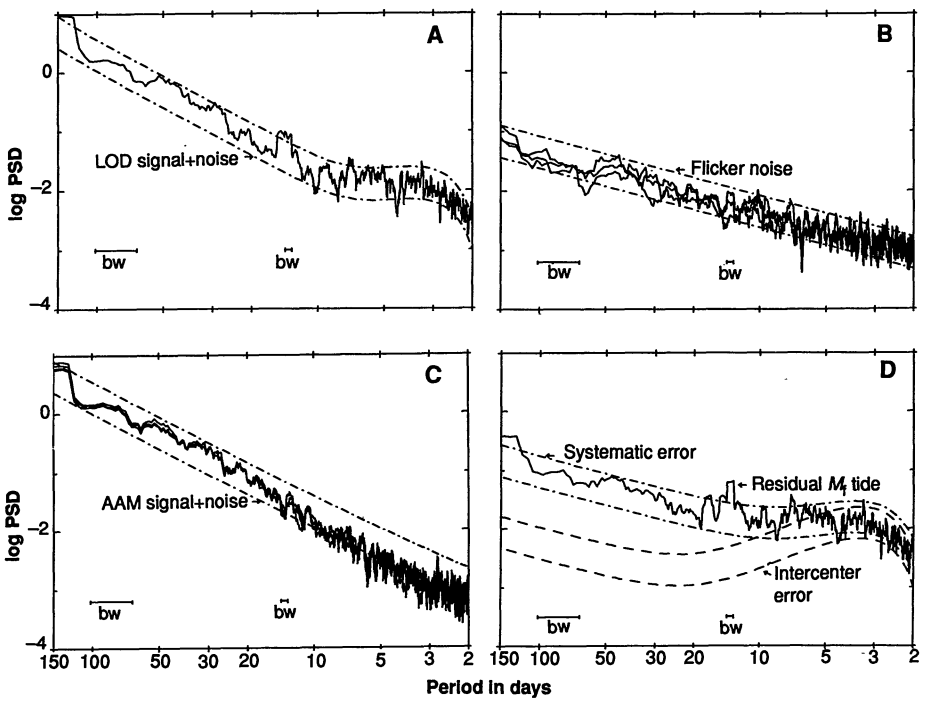

Fig. 3. (**A**) Power spectral density of *LOD** as determined from the IRIS Intensive UT1 measurements (*8*), shown with the 95% confidence band for the expected power based on the model discussed in the text; (**B**) power spectra of the pairwise differences of *AAM* analyses from the JMA, NMC, and UKMO, compared with the 95% confidence band for flicker noise; (**C**) as in (A), for the individual *AAM* analyses from the EC, JMA, NMC, and UKMO; (**D**) PSD of the difference between the LOD_I^* and the combined *AAM* data set, shown with 95% confidence bands for models based on a systematic error common to all *AAM* data sets and on intercenter errors only (see text). Units are milliseconds squared per cycle per day. Smoothing = 11 in all panels.

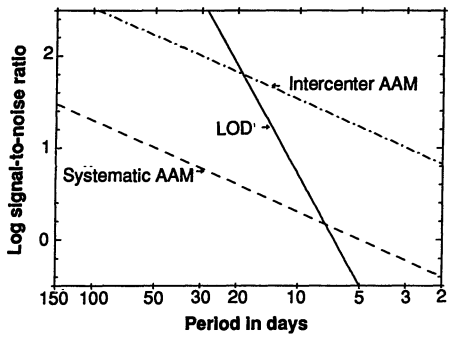

Fig. 4. Signal-to-noise (*SNR*) ratios (in power) specified by the models discussed in the text. The *SNR* values at 10 days are 5.0, 2.0, and 32.8 for the LOD^*_T, systematic *AAM*, and intercenter *AAM* models, respectively. The noise present in the systematic *AAM* may reflect either a common error in the *AAM* series or an unmodeled component of the Earth's angular momentum budget with a flicker-like behavior. The noise in the intercenter *AAM* model reflects the effect of averaging the errors from the four individual centers, which are assumed to be statistically independent in this model.

systematic *UT1* error. Therefore, we conclude that either (i) the *AAM* data sets contain a common systematic error component, or (ii) the Earth's angular momentum budget has an additional component with a flickerlike behavior between periods of about 10 and 100 days.

A systematic *AAM* error would not be surprising, in that all numerical weather prediction centers have access to the same observational meteorological data sets. If we assume that the residual at periods of 10 to 100 days is mostly due to a common *AAM* error, the power in the difference spectrum (Fig. 3D) indicates that the *SNR* is about 2 at a period of 10 days for the averaged *AAM* data; the resulting model for the *PSD* of the residual ("systematic error" in Fig. 3D) gives a reasonable fit over periods from

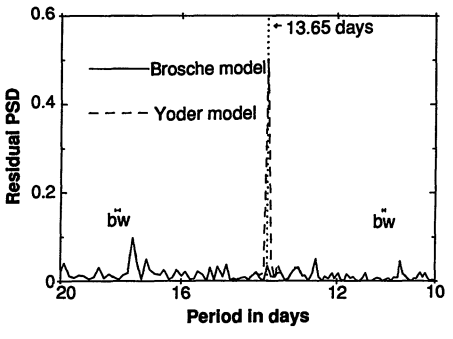

Fig. 5. Power spectral density of the difference between *LOD** as measured by the combined space geodetic techniques and that inferred from a combined *AAM* data set (see text) using the tidal model of Yoder *et al.* [shown as a dashed line (*18*)] and that of Brosche *et al.* [shown as a solid line (*19*)]. Units are milliseconds squared per cycle per day. Smoothing = 1.

150 to 2 days. The transition of the residual power curve at periods below 15 days into a non f^{-1} type behavior suggests that Earth rotation errors dominate at high frequencies, consistent with the estimated *SNR*s for these two data types (Fig. 4).

The largest deviation of the residual power from the systematic error model occurs at 13.6 days, coinciding with the fortnightly tidal band in the residual spectral plot (Fig. 3D). A linear plot of the PSD of the residual between the JPL Kalman-filtered *LOD** and the combined *AAM*, using a periodogram (no smoothing in the frequency domain), shows a sharp peak at 13.65 days (Fig. 5; the 13.63- and 13.66-day tidal lines are not resolved in this spectrum). In developing the current standard model for the tidal terms in *UT1* and *LOD*, Yoder *et al.* (*18*) considered the interaction of the equilibrium ocean tide with the solid Earth; in developing a newer model, Brosche *et al.* (*19*) used a numerical model to calculate the oceanic moment of inertia changes as well as the tidal currents, that is, both the matter and motion terms in the angular momentum of the ocean. Implementing the Brosche model removes the discrepancy in the residuals at the fortnightly period; the nonequilibrium residual at the monthly period is small (*19*), and cannot be detected in our data sets. Significant coherence between the combined *AAM* and JPL Kalman-filtered *LOD** data using the Brosche correction at the 13.6- day period is evident down to 8 days, although there is some indication of a remaining discrepancy at the tidal period (Fig. 2C).

The model incorporating the systematic *AAM* error (Figs. 2 and 3) fits the data reasonably well, and indicates that the loss of significant coherence near 8 days may be due to the decreasing *SNR* present in both data types. The loss of coherence at 8 days, however, is more abrupt than that predicted by either of the models. Clearly, a model taking into account the systematic component is required to explain the observed coherence, in addition to being required to explain the *LOD**-*AAM PSD* (Fig. 3D). The coherence results, like the *LOD**-*AAM PSD* results, cannot be used to distinguish between a systematic error in the *AAM* observations and an additional, unmodeled component of the Earth's angular momentum budget with a flickerlike spectral behavior. For both models the dominance of *LOD* noise at high frequencies (see Fig. 4) indicates that the loss of coherence at periods shorter than 1 week is largely due to measurement error in the Earth rotation data. Improvements in accuracy of geodetic measurements are required to increase the *SNR* and so make it possible to examine the Earth's angular momentum budget at periods shorter than 8 days.

REFERENCES AND NOTES

1. W. H. Munk and G. J. F. MacDonald, *The Rotation of the Earth: A Geophysical Discussion* (Cambridge Univ. Press, New York, 1960); K. Lambeck, *Geophysical Geodesy: The Slow Deformations of the Earth* (Oxford Univ. Press, Oxford, 1988).
2. R. Hide and J. O. Dickey, *Science* **253**, 629 (1991).
3. R. T. H. Barnes, R. Hide, A. A. White, C. A. Wilson, *Proc. R. Soc. London Ser. A* **387**, 31 (1983).
4. R. D. Rosen and D. A. Salstein, *J. Geophys. Res.* **88**, 5451 (1983).
5. T. M. Eubanks, J. A. Steppe, J. O. Dickey, P. A. Callahan, *ibid.* **90**, 5385 (1985).
6. R. D. Rosen, D. A. Salstein, T. M. Wood, *ibid.* **95**, 265 (1990).
7. J. O. Dickey, S. L. Marcus, J. A. Steppe, R. Hide, *Eos* **70**, 1055 (1989); R. D. Rosin, in *Proceedings of the AGU Chapman Conference on Geodetic VLBI: Monitoring Global Chance*, W. E. Carter, Ed. (NOAA Technical Report NOS 137NGS4a, Rockville, MD, 1991).
8. D. S. Robertson, W. E. Carter, J. Campbell, H. Schuh, *Nature* **316**, 424 (1985).
9. D. D. Morabito, T. M. Eubanks, J. A. Steppe, in *The Earth's Rotation and Reference Frames for Geodesy and Geodynamics*, A. K. Babcock and G. A. Wilkins, Eds. (Kluwer Academic, Dordrecht, 1988), pp. 257–268; R. S. Gross and J. A. Steppe, in *IERS Annual Report for 1990*, M. Feissel, Ed. (Observatoire de Paris, Paris, in press).
10. D. A. Salstein, in *International Earth Rotation Service Technical Note 2*, M. Feissel, Ed. (Observatoire de Paris, Paris, 1989), p. 77.
11. K. Arpe, in *ibid.*, p. 81.
12. I. Naito, Y. Goto, N. Kikuchi, in *ibid.*, p. 83.
13. R. Hide, *ibid.*, p. 88.
14. J. O. Dickey, T. M. Eubanks, J. A. Steppe, in *Earth Rotation: Solved and Unsolved Problems*, A. Cazenave, Ed. (*NATO Adv. Inst. Ser. C* **187**, Reidel, Boston, 1986), pp. 137–162.
15. R. D. Rosen and D. A. Salstein, *Mon. Weather Rev.* **115**, 1627 (1985).
16. D. R. Brillinger, *Time Series: Data Analysis and Theory* (Holt, Reinhart and Winston, New York, 1975).
17. Let $\delta\Lambda(t) \equiv \Lambda(t) - \Lambda_o$ and $U(t) \equiv UT1(t) - t$; then to first order in $\delta\Lambda/\Lambda_o$ we have $\delta\Lambda = -\Lambda_o(dU/dt)$ and an estimate of $\delta\Lambda$ is $\widehat{\delta\Lambda} = -\Lambda_o[U(t + \Delta t/2) - U(t - \Delta t/2)]/\Delta t$. The transfer function from U to $\widehat{\delta\Lambda}$ at frequency f is $-\Lambda_o i2\pi f \sin \pi f\Delta t/\pi f\Delta t$ which differs from the transfer function from U to $\delta\Lambda$ by the factor $\sin \pi f\Delta t/\pi f\Delta t$. In practice, the IRIS Intensive *UT1* observations have an availability rate of approximately 68%, resulting in an average spacing of about 1.47 days. Furthermore, *LOD* values are computed at constant (solar) time of day, while the *UT1* determinations on which they are based tend to cluster at constant sidereal times over observational schedules lasting several months. The consequent noncentering of the *UT1* measurements further increases the effective time step for the *LOD* calculation, leading in particular to a doubling of the interval over which *UT1* differences are effectively taken in the extreme case when the *LOD* and *UT1* epochs coincide. Although these operational characteristics are difficult to represent analytically, examination of spectra from the IRIS Intensive data suggests that the overall effect can be roughly accounted for by assuming an interpolation time scale of about 1.75 days in the *LOD* data.
18. C. F. Yoder, J. G. Williams, M. W. Parke, *J. Geophys. Res.* **86**, 881 (1981).
19. P. Brosche, U. Seiler, J. Sundermann, J. Wunsch, *Astron. Astrophys.* **220**, 318 (1989).

20. The authors are grateful to A. P. Freedman and R. S. Gross for useful discussions and their assistance in the data preparation. The work of three of the authors (J.O.D., S.L.M. and J.A.S.) presents the results of one phase of research carried out at the Jet Propulsion Laboratory, California Institute of Technology, under contract with the National Aeronautics and Space Administration.

16 August 1991, accepted 30 October 1991